Accepted Manuscript

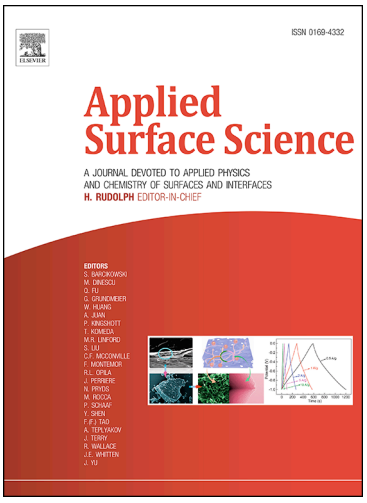

Full Length Article

Polyamide 6.6 separates oil/water due to its dual underwater oleophobicity/underoil hydrophobicity: Role of 2D and 3D porous structures

Pei Zhao, Ning Qin, Carolyn L. Ren, John Z. Wen

PII: S0169-4332(18)32735-1
DOI: https://doi.org/10.1016/j.apsusc.2018.10.041
Reference: APSUSC 40609

To appear in: *Applied Surface Science*

Received Date: 17 July 2018
Revised Date: 28 September 2018
Accepted Date: 4 October 2018

Please cite this article as: P. Zhao, N. Qin, C.L. Ren, J.Z. Wen, Polyamide 6.6 separates oil/water due to its dual underwater oleophobicity/underoil hydrophobicity: Role of 2D and 3D porous structures, *Applied Surface Science* (2018), doi: https://doi.org/10.1016/j.apsusc.2018.10.041

Polyamide 6.6 separates oil/water due to its dual underwater oleophobicity/underoil hydrophobicity: Role of 2D and 3D porous structures

Pei Zhao, Ning Qin, Carolyn L. Ren, John Z. Wen*
Department of Mechanical and Mechatronics Engineering, University of Waterloo, 200 University Avenue West, Waterloo, Ontario, N2L 3G1, Canada
*E-mail: john.wen@uwaterloo.ca

Keywords: Polyamide 6.6, meshes and nonwoven fabrics, oil/water separation, intrusion pressure and contact angle, dual underwater oleophobicity and underoil hydrophobicity

Abstract
Porous polyamide functionalized by plasma or various coatings has been investigated for oil/water separation. In literature, polyamide has rarely been studied for oil removal. This work investigated the performance of bare polyamide 6.6 (nylon 6.6) in terms of the oil/water separation efficiency and the intrusion pressure, inspiring cost-effective solutions for large-scale oil removal in the industry. Both polyamide meshes possessing two-dimensional (2D) one-layer pores and nonwoven fabrics with three-dimensional (3D) irregular pores were found to be able to separate oil/water with a high efficiency above 98.5%. This finding was attributed to the dual underwater oleophobicity and underoil hydrophobicity of these polyamide samples. The roles of 2D and 3D structures in oil/water separation were illustrated, to provide a new insight into filter designing. Thanks to its greater intrusion pressure, the 3D netting structure was suggested being more beneficial for oil/water separation than the 2D structure.

1. Introduction

Oil/water separation has been a global environmental challenge because of the production of industrial oily wastewater and frequent occurrences of oil spill accidents. For example, the oily wastewater loading at a typical mining site is around 140kL/day [1]. Mechanical techniques, such as gravity separation, skimming, and flotation, are employed to recover oil in industry, which have disadvantages of high cost and low efficiency [2]. Sorbents are also used to remove oil through soaking up oil, including natural organic (straw, sawdust), natural inorganic (vermiculite, pumice) and synthetic materials (polypropylene), but limited by their low selectivity, low capacity and poor recyclability [3]. Recently, advanced sorbents with superoleophilicity and superhydrophobicity, such as P(St-DVB)/Fe3O4 microspheres, have been developed [4,5]. Alternatively, metal and polymer meshes/membranes coated by novel materials are used as filters to separate oil and water, allowing one to flow through while resisting the other. Those coatings exhibit distinct wettability to water and oil, 1) hydrophobicity and oleophilicity simultaneously [6,7], 2) underwater oleophobicity [8-13], or 3) hydrophobicity in oil [10], of which the second introduces fouling resistance [11]. In addition, a special filter design using a porous Janus membrane, which has a hydrophobic/hydrophilic asymmetry, has drawn much research attention [14,15]. These advanced filters are able to separate oil and water with high efficiency, high selectivity and good recyclability at a lab scale. Scaling up and cost evaluation are required for industrial applications of the advanced filters.

One way to realize large-scale oil/water separation in the industry is to use proper economic materials. Polyamide 6.6 (nylon 6.6) is a commercial material that can be readily used in a large scale. Porous polyamide meshes/membranes coated with various materials that have special wettability, such as polydopamine and polydivinylbenzene, have been developed for oil removal [16-18]. In addition, polyamide meshes functionalized by atmospheric pressure plasma, showing a satisfying underwater oleophobicity, effectively separated oil/water [19]. Recently, spunbond nylon 6,6 nonwoven fabrics without any treatment were used as first responders for oil spills both in Eucutta and in New Augusta, Mississippi, to absorb oil and prevent further contamination [20]. This nonwoven nylon was characterized by its manufacturer regarding separating oil from oil-in-water emulsion [20]. It trapped oil within the fabric but allowed water to flow through its pores [20].

To develop economic polyamide 6.6 for large-scale oil/water separation, knowledge gaps remain, such as why nonwoven polyamide 6.6 can effectively separate oil/water, whether polyamide 6.6 meshes are capable of oil removal, and whether different porous structures of polyamide influence the oil/water separation. One important property to characterize the oil/water separation performance is the intrusion pressure of oil (or water), representing the robustness and the capacity of the filter. The intrusion pressure closely relates to the oil (or water) contact angle (CA) of the filter [21], which depends on the surface energy and microstructure of the filter [22-24]. Meshes and nonwoven fabrics show different microstructures, two-dimensional (2D) one-layer orderly porous structure and three-dimensional (3D) irregular porous structure, respectively, which could lead to their different oil removal performances. A systematic study of polyamide 6.6 2D meshes and 3D nonwoven fabrics for oil/water separation is hence needed, to address the aforementioned questions and to extend the use of polyamide 6.6 in the oil removal industry. In this work, polyamide 6.6 2D meshes and 3D nonwoven fabrics were investigated to correlate their microstructures and oil/water separation properties. The oil/water separation efficiency and the intrusion pressure were measured and elaborated, to illustrate the effects of the dual underwater oleophobicity and underoil hydrophobicity during oil/water separation. The research findings are expected to provide an insight into potential applications of cost-effective polyamide 6.6 in the large-scale oil removal industry.

2. Experimental

2.1 Materials

Polyamide 6.6 (nylon 6.6) meshes were purchased from Component Supply, Tennessee. Polyamide 6.6 nonwoven fabrics (thermal bonded, PBN-II®, Type 30) were provided by Cerex Advanced Fabrics, Florida. Heavy mineral oil, dopamine hydrochloride (DA), TEOS, chloroform, oil red, methyl orange, and ammonia solution (concentration 28-30%) were bought from Sigma-Aldrich, Canada.

2.2 Oil/water separation

In oil/water separation experiments, a piece of polyamide 6.6 (7cm×7cm) or seven layers of stacked polyamide 6.6 meshes were fixed under a tube with a clamp (see supporting information fig. S1) to form a filter. Water was fed into the tube to prewet the polyamide 6.6. Then a mixture of heavy mineral oil dyed with oil red and water (1:1, 20ml) was poured into the tube. The filtrated water was collected to evaluate the separation efficiency η, defined by $(1\text{-}C_1)\times100\%$, where C_1 is the oil concentration in water after the separation. C_1 was measured by UV-Vis spectrometer (the details are in the supporting information). The water flux (v) was calculated by the equation of $v=V/St$, where V is the volume of the collected water, S is the surface area of the filter and t is the time used for collecting the water. The intrusion pressure (P_{intru}) of oil was measured by keeping adding oil into the tube till the maximum height (h_{max}), when oil started to penetrate the polyamide 6.6, according to $P_{intru}= \rho_{oil}\, g\, h_{max}$. For separating water and chloroform that is heavier than water (1;1, 20ml), the polyamide 6.6 was prewetted by heavy mineral oil (not by chloroform that is vaporized fast and cannot keep the polyamide 6.6 wet). The separated chloroform was collected for the evaluation of the separation efficiency η, which was defined by $(1\text{-}C_2)\times100\%$, where C_2 is the water concentration in the filtrated chloroform (supporting information). And the intrusion pressure of water was calculated by $P_{intru}= \rho_{water}\, g\, h_{max}$.

2.3 Characterization

The morphologies and microstructures of the samples were observed by using an Atomic Force Microscopy (AFM, MultimodeTM SPM, Digital Instruments) in a tap mode and a SEM (Zeiss ULTRA Plus). CAs including water contact angle (WCA), oil contact angle in water (O/W) and water contact angle in oil (W/O) were measured using a lab-made contact angle meter, set up by a syringe needle, a side-view microscope, and a camera.

3. Results and Discussion

Polyamide 6.6 meshes with a pore size of 25, 64, 85, 112, and 155μm, denoted as mesh_25, mesh_64, mesh_85, mesh_112, and mesh_155, and nonwoven fabrics with a density of 1, 2, 3 and 4 ounces per square yard, expressed as nonwoven_1, nonwoven_2, nonwoven_3, and nonwoven_4, were investigated in this work. The diameter of the yarn/wire and the open area (pore area/total area) of the meshes were shown in supporting information table S1.

Microstructures of mesh_64 and nonwoven_4 are shown in fig. 1, as examples of polyamide 6.6 meshes and nonwoven fabrics. The meshes presented one layer of ordered square pores (2D), while the nonwoven fabrics had layered irregular pores (3D) whose size was difficult to be determined due to the irregularity. With the increase of the density of the nonwoven fabric, the average pore size gets smaller under the optical microscope. The densest nonwoven polyamide 6.6 in this work, nonwoven_4, was considered to have an average size of 68±33μm [20]. Once the polyamide 6.6 samples were prewetted by water or oil, they were able to separate mixtures of water and oil (fig. 2-a-b) due to their underwater oleophobicity and underoil hydrophobicity proved by their O/W and W/O (fig. 2-c-d). The error bars here and in the following figures were the standard deviations.

When polyamide 6.6 was prewetted by water, it allowed water to drip through its pores but blocked the heavy mineral oil by oil/water interfacial tension (figure 2-a). To separate water and chloroform that is heavier than water, polyamide 6.6 was prewetted by oil, which allowed chloroform to penetrate but resisted water (figure 2-b). The separation process was driven by gravity. As shown in fig. 3, the separation efficiencies of all the polyamide 6.6 samples were higher than 98.5%, the efficiency of polyamide 6.6 prewetted by water was slightly higher than that prewetted by oil, and the efficiency had the trend to decrease with increasing the pore size of the mesh (with decreasing the density of the nonwoven). Fig. 4 shows the intrusion pressures of oil and water for all polyamide 6.6 samples. The intrusion pressure increased with the decrease of the pore size of polyamide 6.6 mesh and with the increase of the density of the nonwoven fabric. Especially, as shown in fig. 4-a, when several (7) layers of meshes were stacked together to be tested, the intrusion pressure was one or two times higher than that of one mesh. However, the water flux (fig. S6) that represents the separation speed declined with decreasing the pore size of polyamide 6.6, and was particularly slow for the densest nonwoven_4 and stacked meshes_25. An optimal balance between the intrusion pressure (the separation capacity and the robustness) and the water flux (the separation speed) would be required for practical applications.

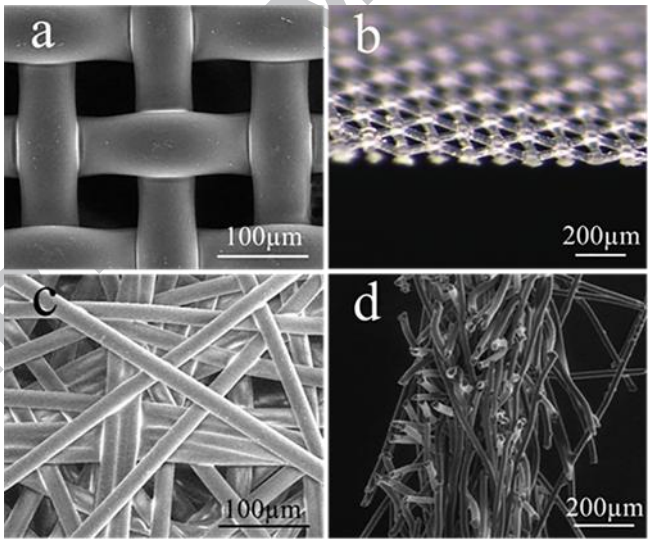

Fig. 1. Scanning Electron Microscope (SEM) images of top and side views of as-purchased polyamide 6.6 mesh_64 (a, b) and nonwoven_4 (c, d). The mesh has a 2D ordered pore structure (a, b) and the nonwoven has 3D disordered pores (c, d).

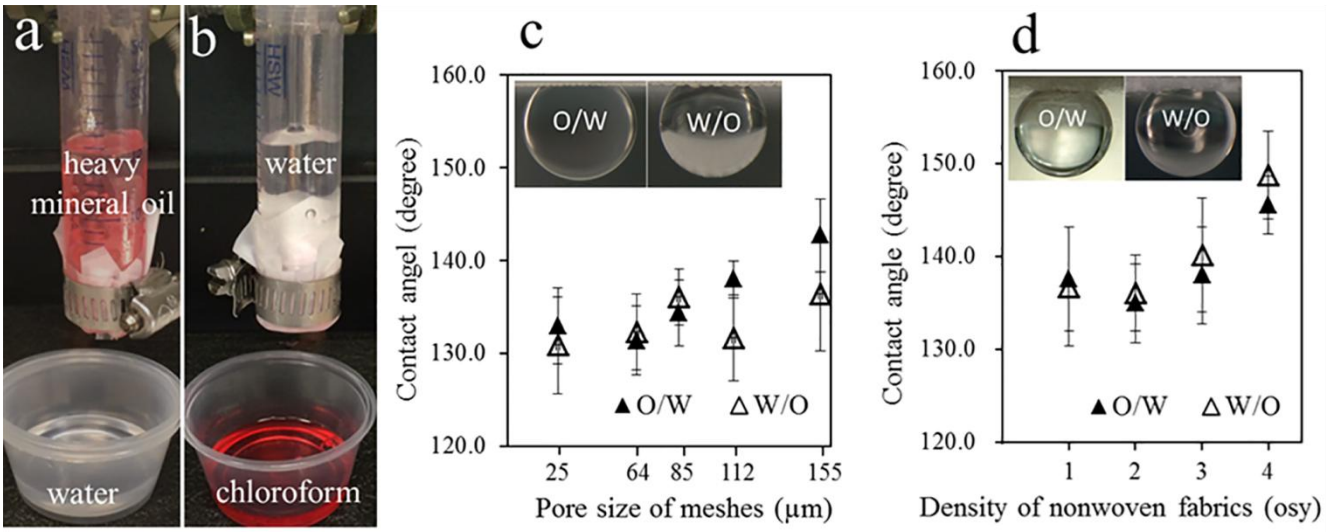

Fig. 2. Polyamide 6.6 mesh_64 prewetted by water (a) or by heavy mineral oil (b) successfully separated water and oil, so did the other polyamide 6.6 samples. Heavy mineral oil contact angle in water (O/W) and water contact angle in heavy mineral oil (W/O) of polyamide 6.6 meshes (c) and nonwoven fabrics (d). The insets in fig. (c) and (d) are images of contact angles of mesh_64 and nonwoven_2.

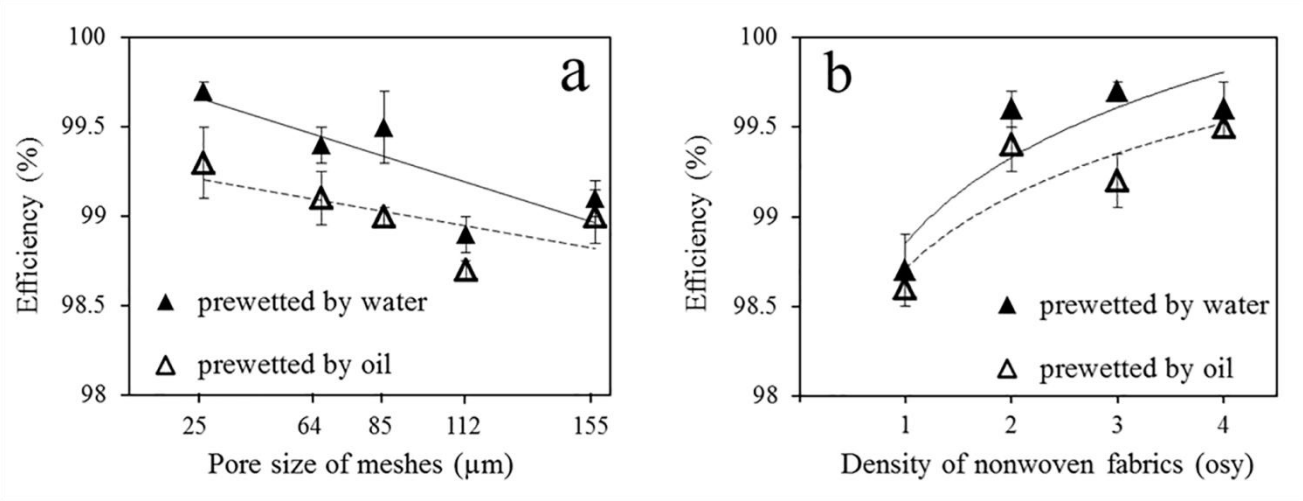

Fig. 3. The separation efficiencies of polyamide 6.6 meshes (a) and nonwoven fabrics (b) prewetted by water or oil. The solid and dotted lines are the trend lines for the efficiency of polyamide 6.6 prewetted by water and oil, respectively.

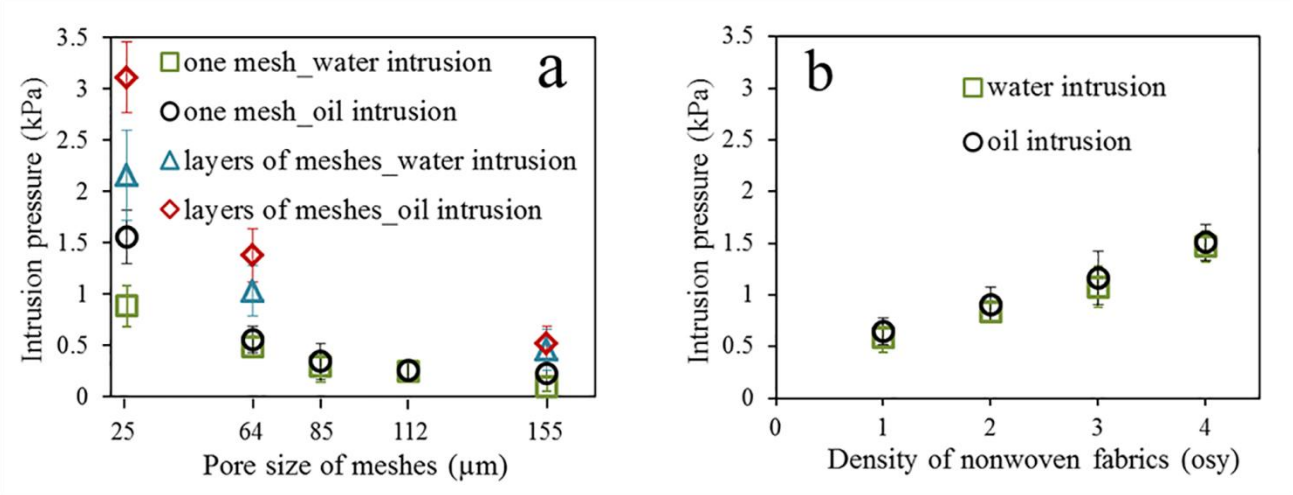

Fig. 4. The experimental intrusion pressures of heavy mineral oil and of water for polyamide 6.6 meshes (a) and nonwoven fabrics (b). Oil intrusion means the intrusion pressure of heavy mineral oil for polyamide 6.6 prewetted by water. Water intrusion represents the intrusion pressure of water for polyamide 6.6 prewetted by heavy mineral oil.

The mesh and nonwoven were modified by using the same method to verify whether the improvement of the intrusion pressure would be the same or different for the 2D and 3D samples. Surface coating [25] and plasma treatment were used to improve the intrusion pressure of oil for polyamide 6.6 mesh_64 and nonwoven_2. The details of the treatment procedures are presented in the supporting information. The method to enhance the intrusion pressure of water wasn't investigated here, as most types of oil is lighter than water and to separate those oil from water polyamide 6.6 prewetted by water should be used. The theoretical intrusion pressure of oil (or of water) for a filter is given in equation (1), where γ_{ow} is oil/water interfacial tension, $\theta_{O/W}$ (or $\theta_{W/O}$) is the value of O/W (or W/O) and d is the pore size [21, 26-28].

$$P_{intru} = -\frac{2\gamma_{ow}\cos\theta_{O/W}}{d} \quad (\text{or } P_{intru} = -\frac{2\gamma_{ow}\cos\theta_{W/O}}{d}) \tag{1}$$

Therefore, the intrusion pressure of oil could be improved by increasing the O/W, which is determined by the surface chemistry and the roughness of the filter [22-24]. For a perfect surface without any roughness, the relation of O/W and WCA follows equation (2), where θ_w is the value of WCA and γ_o (or γ_w)is the surface tension of oil (or water) [22,29].

$$\theta_{O/W} = 180° - \arccos\left[\frac{2(\cos\theta_w - 1)}{1 - \frac{\gamma_o - \gamma_{ow}}{\gamma_w}} + 1\right] \tag{2}$$

Equation (2) indicates that $\theta_{O/W}$ increases with the decrease of θ_w. In addition, the CA is affected by the surface roughness according to Wenzel ($\cos\theta = r\cos\theta_Y$) or Cassie ($\cos\theta = f(\cos\theta_Y + 1) - 1$) models, where θ is measured or apparent CA on the real rough surface, θ_Y is Young CA on the ideal flat surface, r is the ratio of the actual over the projected surface area and f is the fraction of solid surface in contact with the droplet [22,24,30-33]. The O/W of polyamide 6.6 that is larger than 90^0 could increase with the increase of roughness. Therefore, in order to increase O/W and improve the intrusion pressure for polyamide 6.6, we used two modification strategies, coating superhydrophilic polydopamine/tetraethyl orthosilicate (PDA/TEOS) on the polyamide 6.6 surface and etching the polyamide 6.6 surface by using oxygen plasma to create a large roughness.

Microstructures of as-purchased, PDA/TEOS coated, plasma treated polyamide 6.6 mesh_64 and nonwoven_2 are shown in fig. 5 and fig. S7, respectively. The as-purchase polyamide 6.6 had a smooth surface, PDA/TEOS particles were successfully coated on the surface and a rough surface was achieved by using plasma treatment. Due to the superhydrophilicity of PDA/TEOS, WCA of the coated polyamide 6.6 was zero comparing to ~90^0 of the original mesh and ~65^0 of the original nonwoven fabric (fig. 5-d and fig. S7-d). The surface roughness of the mesh_64 samples was determined by AFM analysis as shown in fig. 6 and table S2. Both the coated (Ra=88.2±7.9nm, r=1.28±0.08) and plasma treated (Ra=206.9±84.6nm, r=1.44±0.07) meshes had a large roughness, much larger than the original mesh (Ra=13.9±1.5

nm, r= 1.07±0.02). Then the coating process brought in the modified surface chemistry as well as the rougher surface. Consequently, as shown in fig. 7, compared to the original polyamide 6.6, both the coated and plasma treated samples showed increased O/W and improved intrusion pressure of oil, where the improvement caused by the coating process was slightly larger than that resulted from the plasma treatment.

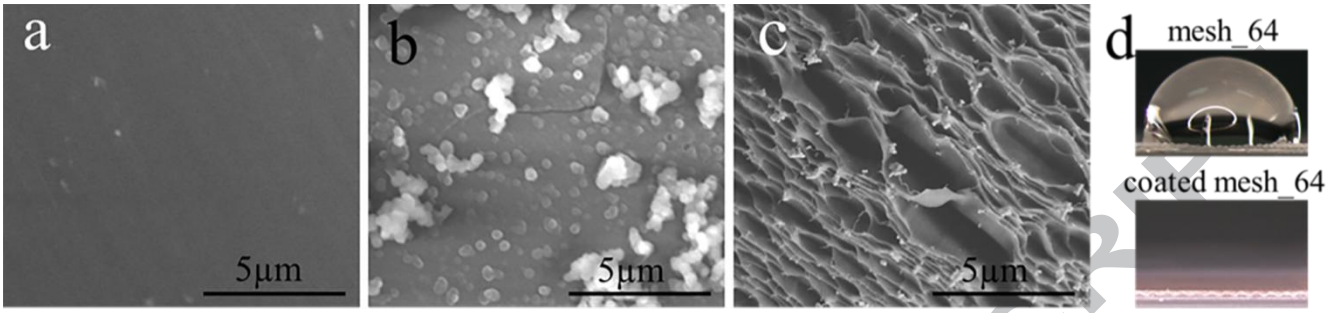

Fig. 5. SEM images of as-purchased (a), PDA/TEOS coated (b) and plasma treated (c) polyamide 6.6 mesh_64. Water contact angle in air of as-purchased and PDA/TEOS coated mesh_64 (d).

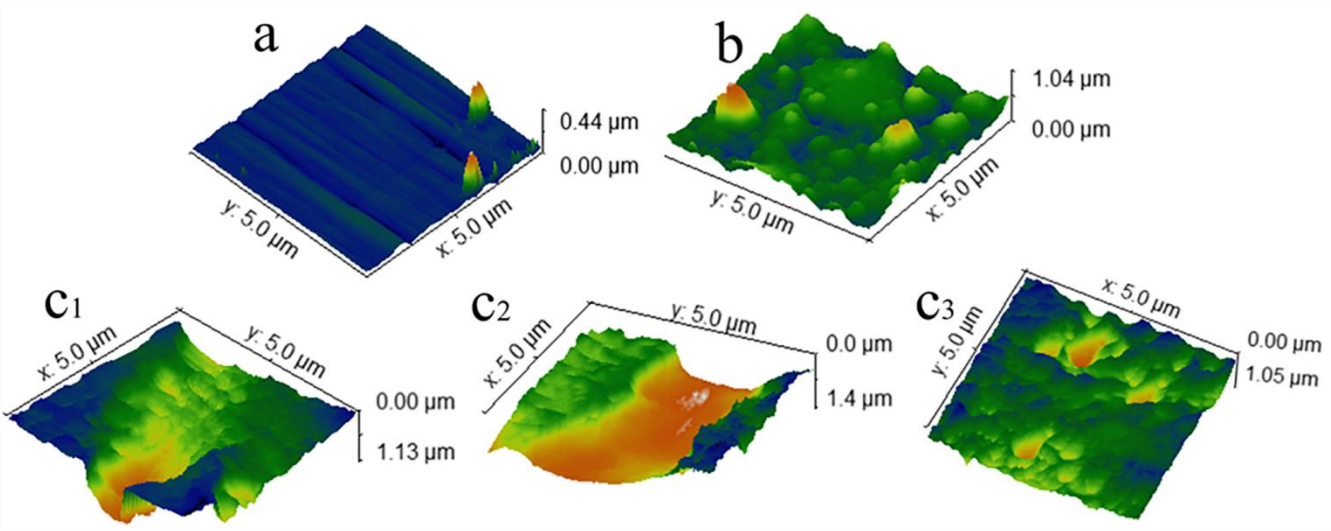

Fig. 6. AFM images of the surfaces of as-purchased (a), PDA/TEOS coated (b) and plasma treated (c) polyamide 6.6 mesh_64. The grooves on the plasma treated polyamide 6.6 mesh_64 were not homogeneous, consistent with fig. 5-c, and thus three representative AFM images are given in fig. 6-c.

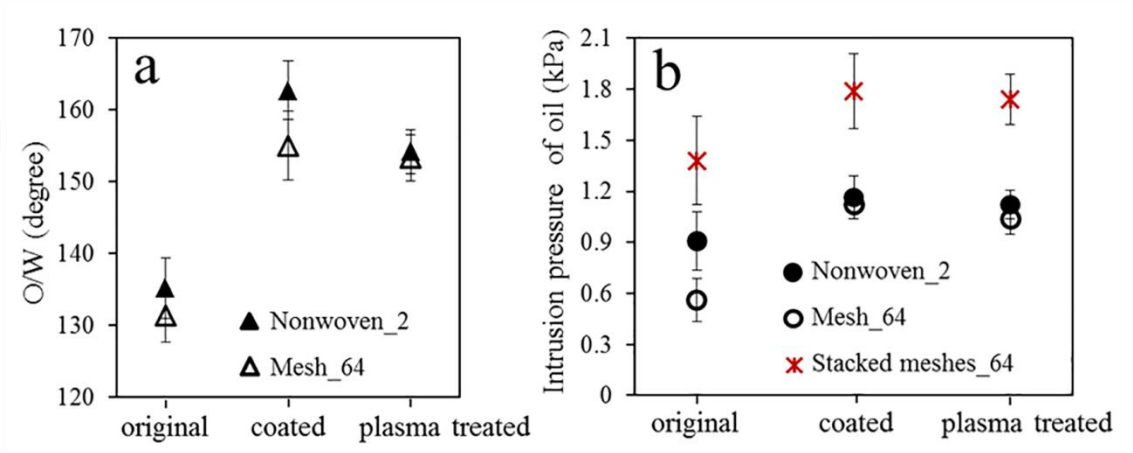

Fig. 7. The oil contact angle in water (O/W) (a) and the experimental intrusion pressures of oil for original, PDA/TEOS coated and plasma treated polyamide 6.6 mesh_64 (hollow symbols) and nonwoven_2 (solid symbols). The red star symbols are the intrusion pressures for stacked layers of meshes_64.

It is worth noting that for the mesh and nonwoven fabric, the same modification methods resulted in a similar increase of O/W from ~130^0-135^0 to ~150^0-160^0 (fig. 7-a), but quite different degrees of improvement of intrusion pressure, from ~0.5kPa to ~1.1kPa (doubled) for the mesh and from ~0.9kPa to ~1.1kPa (30% higher) for the nonwoven (fig. 7-b). For the stacked meshes_64, the average intrusion pressure was enhanced from ~1.38kPa to ~1.75kPa after the surface modification, also around 30% higher like the nonwoven (fig. 7-b). The different degrees of intrusion pressure improvement for the mesh and the nonwoven (or the stacked meshes) were caused by their respective 2D and 3D pore structures, which could lead to different contact modes of oil and water within the pores.

Schematics of the contact of oil and water within a pore of the polyamide 6.6 samples under the intrusion pressure were depicted in fig. 8. Layers of stacked meshes had irregular 3D pores like the nonwoven. The irregular pore structure was simplified to be a regular 3D one in the schematic. To determine the intrusion pressure of oil by equation (1) for the nonwoven and stacked meshes, the O/W is supposed to be that on a row of wires, which was assumed to be similar with the measured O/W on the nonwoven and mesh surfaces ($\theta_{nonwoven\_O/W}$ and $\theta_{mesh\_O/W}$) that are composed of rows of wires. Due to their irregular pore structures, the pore size was not homogeneous and difficult to be determined, and then the theoretical intrusion pressure could not be calculated. However, comparing to the original samples, the enhancement of the theoretical intrusion pressure for the modified ones was supposed to be proportional to the increase of $cos\theta_{nonwoven\_O/W}$ or $cos\theta_{mesh\_O/W}$, which was measured to be ~1.35 ($\cos162^0/\cos135^0$ = -0.951/-0.706), 1.27 ($\cos154^0/\cos135^0$ = -0.898/-0.706), 1.37 ($\cos155^0/\cos131^0$ = -0.906/-0.66) and 1.34 ($\cos153^0/\cos131^0$ = -0.89/-0.66) for the coated nonwoven, plasma treated nonwoven, coated stacked meshes and plasma treated stacked meshes, respectively, as indicated in fig. 7-a. Therefore, the theoretical improvement of the intrusion pressure, 27%-37% for the modified nonwoven and stacked meshes, was roughly consistent with the measured improvement, around 30% as shown in fig. 7-b (solid and star symbols).

For the 2D mesh, the O/W on a wire ($\theta_{wire\_O/W}$) should be used to determine the intrusion pressure, not the measured O/W on the mesh surface (the wire was woven to the mesh). The CAs on a wire and on a mesh were depicted in fig. 8-c, as the topography affects the CA. The O/W on the wire was difficult to be measured but could be calculated by the measured O/W on the mesh according to equation (3), where R is the radius of the wire and d is the pore size of the mesh [23,24].

$$\cos\theta_{mesh} = -1 + \frac{R}{R+\frac{d}{2}}[\sin\theta_{wire} + (\pi - \theta_{wire})\cos\theta_{wire}] \quad (3)$$

Thus the O/W on a wire of the original, coated and plasma treated meshes was calculated to be 111^0, 132^0 and 129^0, respectively. The W/O on a wire of the original mesh was 105^0. By using the calculated O/W (or W/O) on the wire, the theoretical intrusion pressure for the polyamide 6.6 mesh was determined by equation (1), which fits very well with the measured data shown in fig. 9. Comparing to the as-purchased mesh_64, the $cos\theta_{wire\_O/W}$ of the coated and plasma treated mesh was almost twice as large ($\cos132^0/\cos111^0$=-0.668/-0.357=1.87 and $\cos129^0/\cos111^0$=-0.628/-0.357=1.78). Thus the theoretical intrusion pressure for the mesh was around doubled after the modifications, consistent with the measured results in fig. 7-b (hollow symbols). Comparing to one mesh, the stacked meshes had smaller or equal irregular pores and the intrusion pressure determined by the measured O/W on the mesh (~135^0) was doubled or even tripled ($\frac{2\gamma_{OW}\cos 135^0}{d_1}$ / $\frac{2\gamma_{OW}\cos 111^0}{d_2} = 1.98\frac{d_2}{d_1}$, where d_1 and d_2 are the pore sizes of the stacked meshes and of the mesh), consistent with the experimental data in fig. 4-a. That means a 3D netting structure of polyamide 6.6 is beneficial for the use of oil/water separation than a 2D mesh structure in terms of the intrusion pressure.

Researchers have developed novel coatings on meshes or membranes for applications of oil/water separation [27,34]. They also coated flat surfaces such as silicon wafers and used the CAs on the coated flat surfaces to calculate theoretical

intrusion pressures for the coated meshes according to equation (1) [27]. The measured and calculated intrusion pressures were fitted well. Because of the same coating procedures, the topography and the CA on the coated flat surface should be the same as those on the coated wire. Our method to determine the theoretical intrusion pressure of a mesh using the CA on the wire, which is calculated by the measured CA on the mesh, is also valuable, especially for the as-purchased meshes, since it is difficult to duplicate a flat surface that has the same texture with the wire surface.

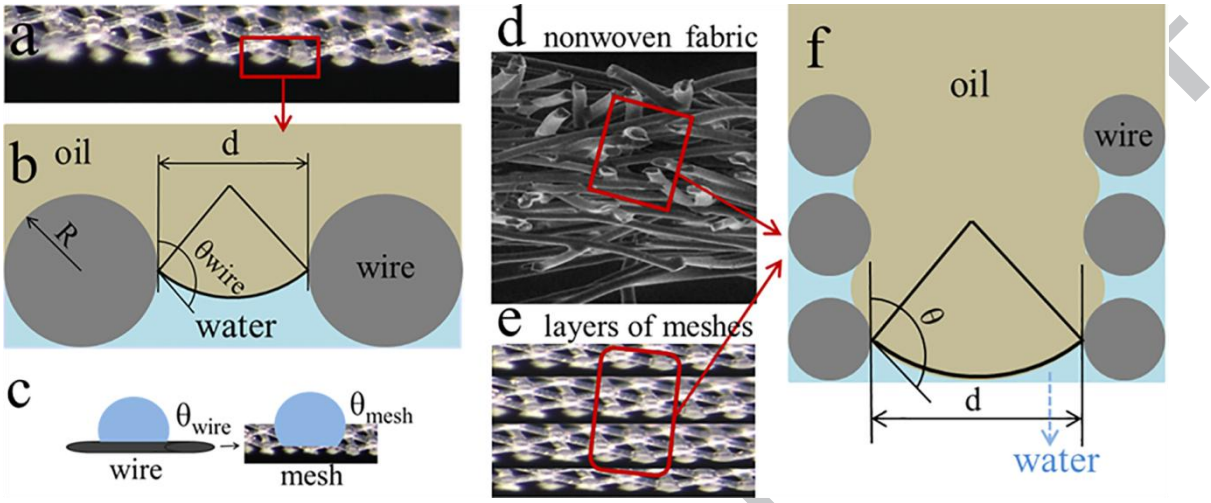

Fig. 8. Side views of the mesh (a), the nonwoven fabric (d) and the stacked meshes (e), schematics of the contact of oil and water under the intrusion pressure within a pore of the mesh (b), the nonwoven fabric or the stacked meshes (f), the contact angles on a wire and on a mesh (c).

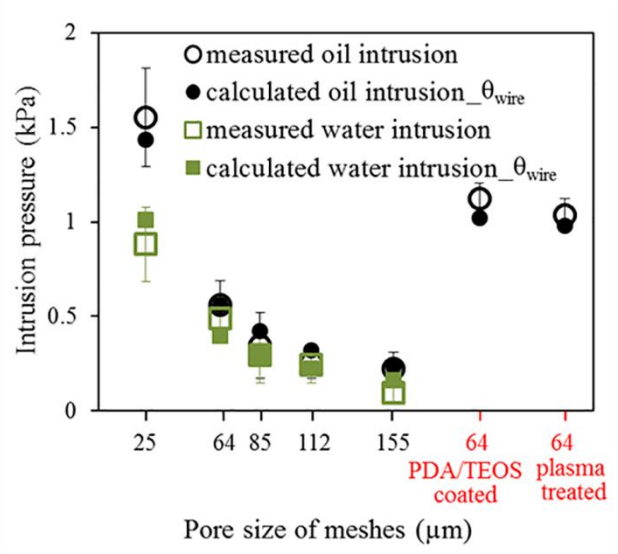

Fig. 9. Comparison of the measured and calculated intrusion pressures for the polyamide 6.6 meshes. The left five points on the X axis are original polyamide 6.6 samples and the right two points that are highlighted by red are modified polyamide 6.6 samples. The theoretical values were calculated by using the contact angle on the wire (θ_{wire}).

The dual underwater oleophobic and underoil hydrophobic properties of the wire, the mesh and the nonwoven resulted from a metastable Cassie state. For an ideal surface, O/W and W/O add up to 180^0. A roughness could even enhance the lyophilicity or the lyophobicity according to Wenzel or Cassie models in a stable state. However, a metastable Cassie state that resulted from proper topography and chemical composition offers access to dual underwater oleophobicity and underoil hydrophobicity [22]. To reach the metastable Cassie regime by designing a surface topography, such as micro grooves or pillars, the lyophilic surface could transform to be lyophobic [22,24,33,35-37]. Metastable states are likely to

correspond to a minimum local free energy [24,38,39]. By applying a force above a threshold, the droplet could penetrate into the micro grooves of the surface and the metastable Cassie state (lyophobic) could be turned to Wenzel (lyophilic) [28,33,37], which corresponds to the minimum global energy. Fig. 10 shows the apparent CAs verses Young CAs in the stable Wenzel/Cassie and metastable Cassie regimes [28,33,39,40]. Ideal polyamide 6.6 surfaces could be oleophilic in water ($\theta_{o/w}$ on a nylon membrane = 88.7^0) [12], which was transformed to underwater oleophobicity on the rough polyamide 6.6 wire (fig. 6-a: there were grooves on the wire surface) according to the metastable Cassie mode. Therefore, the wire of the polyamide 6.6 sample had the dual underwater oleophobicity (111^0) and underoil hydrophobicity (105^0) due to the combined effects of its surface composition and roughness. The meshes and the nonwoven fabrics showed even higher underwater oleophobicity (~130^0-145^0) and underoil hydrophobicity (~130^0-145^0) due to their two levels of roughness: (1) the rough topography on the wires and (2) the uneven surfaces formed when wires are woven to the meshes or bonded to the nonwoven.

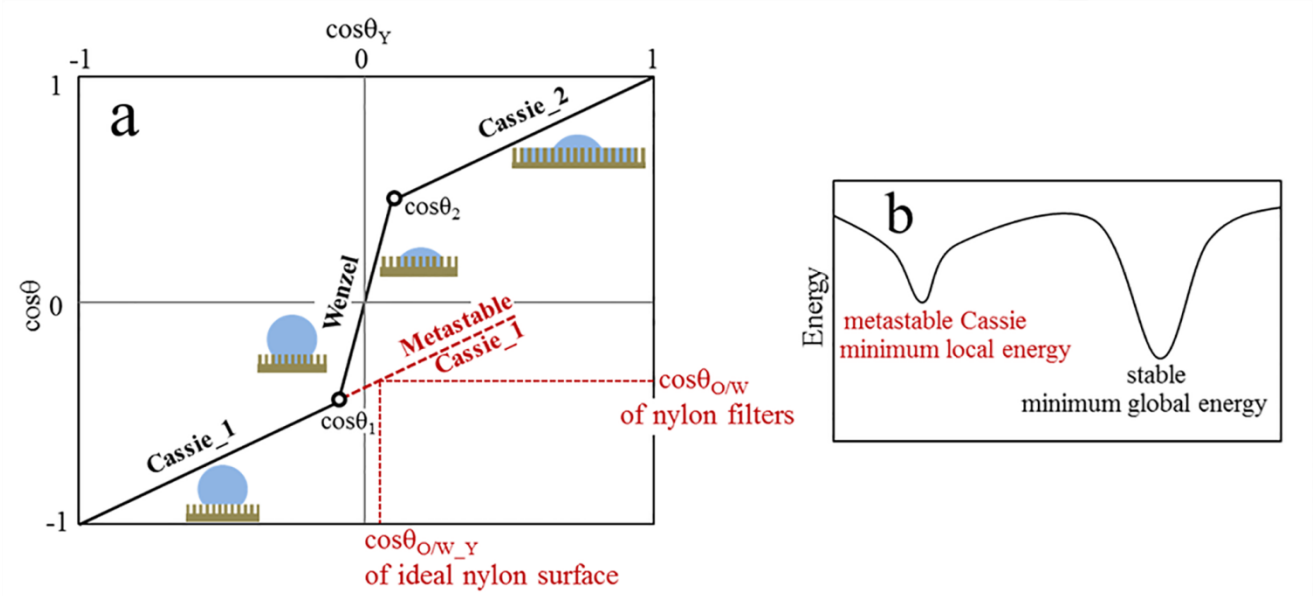

Fig. 10. (a) Relationship between the apparent contact angles θ on structured surfaces and the Young contact angles θ_Y on ideal surfaces in different wetting modes: Cassie_1 regime - The droplet does not penetrate into the surface texture and $\cos\theta = f(1+\cos\theta_Y) - 1$ [28,33,39]; Wenzel regime - The drop fills the grooves of the surface and $\cos\theta = r\cos\theta_Y$ [28,33,39]; Cassie_2 state - A drop and a film of the liquid invade the solid texture and $\cos\theta = f(-1+\cos\theta_Y) + 1$, where f is the fraction of the solid in contact with the drop [40], and $\cos\theta_1$ and $\cos\theta_2$ are determined by the surface texture and defined by $\frac{f-1}{r-f}$ and $\frac{1-f}{r-f}$, respectively. For general surfaces with textures, f may depend on θ_Y and $\cos\theta$ may not a linear function of $\cos\theta_Y$ [24]. (b): The energy at a metastable Cassie state is locally lowest while the stable mode corresponds to the globally minimum energy.

4. Conclusions

This work provides insight into using cost-effective polyamide 6.6 for oil/water separation or as first responders in occurrences of oil spills. Even though polyamide functionalized by various coatings has been developed for oil/water separation, unmodified polyamide has been rarely studied. We verified that two types of polyamide 6.6 filters, which were meshes with a 2D porous structure and 3D nonwoven fabrics, were both able to separate oil/water with a high efficiency of >98.5%, and found out the reason to be the dual underwater oleophobicity and underoil hydrophobicity. For oil/water separation, different CAs at the oil/water/polyamide interface determined the intrusion pressures of 2D and 3D polyamide 6.6. The effective CAs were found to be the CA on the wire surface (not the CA on the mesh surface) for the 2D mesh (the

wire is woven to the mesh) and the CA on the nonwoven surface for the 3D nonwoven, respectively. A 3D netting structure was more beneficial for oil/water separation than a 2D structure in terms of the intrusion pressure.

Acknowledgments

This work was financially supported by the Natural Sciences and Engineering Research Council (NSERC). The authors would like to thank MW Canada Ltd. and especially Lindsay Barber for technical discussions and support.

References

[1] T.F. Guerin, Heavy equipment maintenance wastes and environmental management in the mining industry, J. Environ. Manage. 66 (2002) 185-199.

[2] P.C. Cheng, Z.K. Xu, Mineral-coated polymer membranes with superhydrophilicity and underwater superoleophobicity for effective oil/water separation, Sci. Rep. 3 (2013) 2776.

[3] Use of sorbent materials in oil spill response. Technical information paper, ITOPF, London, United Kingdom.

[4] J. Mao, W. Jiang, J. Gu, S. Zhou, Y. Lu, T. Xie, Synthesis of P (St-DVB)/Fe3O4 microspheres and application for oil removal in aqueous environment, Appl. Surf. Sci. 317 (2014) 787-793.

[5] J. Gao, X. Song, X. Huang, L. Wang, B. Li, H. Xue, Facile preparation of polymer microspheres and fibers with a hollow core and porous shell for oil adsorption and oil/water separation, Appl. Surf. Sci. 439 (2018) 394-404.

[6] G. Ren, Y. Song, X. Li, Y. Zhou, Z. Zhang, X. Zhu, A superhydrophobic copper mesh as an advanced platform for oil-water separation, Appl. Surf. Sci. 428 (2018) 520-525.

[7] H. Cao, W. Gu, J. Fu, Y. Liu, S. Chen, Preparation of superhydrophobic/oleophilic copper mesh for oil-water separation, Appl. Surf. Sci. 412 (2017) 599-605.

[8] Z. Wang, S. Ji, J. Zhang, F. He, Z. Xu, S. Peng, Y. Li, Dual functional membrane with multiple hierarchical structures (MHS) for simultaneous and high-efficiency removal of dye and nano-sized oil droplets in water under high flux, J. Membr. Sci. 564 (2018) 317-327.

[9] Z. Wang, S. Ji, J. Zhang, Q. Liu, F. He, S. Peng, Y. Li, Tannic acid encountering ovalbumin: a green and mild strategy for superhydrophilic and underwater superoleophobic modification of various hydrophobic membranes for oil/water separation, J. Mater. Chem. A 6 (2018) 13959-13967.

[10] D. Qian, D. Chen, N. Li, Q. Xu, H. Li, J. He, J. Lu, TiO_2/sulfonated graphene oxide/Ag nanoparticle membrane: In situ separation and photodegradation of oil/water emulsions, J. Membr. Sci. 554 (2018) 16-25.

[11] Z. Wang, S. Ji, F. He, M. Cao, S. Peng, Y. Li, One-step transformation of highly hydrophobic membranes into superhydrophilic and underwater superoleophobic ones for high-efficiency separation of oil-in-water emulsions, J. Mater. Chem. A 6 (2018) 3391-3396.

[12] H. Zhu, P. Guo, Z. Shang, X. Yu, Y. Zhang, Fabrication of underwater superoleophobic metallic fiber felts for oil-water separation, Appl. Surf. Sci. 447 (2018) 72-77.

[13] K. Hou, Y. Zeng, C. Zhou, J. Chen, X. Wen, S. Xu, J. Cheng, Y. Lin, P. Pi, Durable underwater superoleophobic PDDA/halloysite nanotubes decorated stainless steel mesh for efficient oil–water separation, Appl. Surf. Sci. 416 (2017) 344-352.

[14] Z. Wang, X. Yang, Z. Cheng, Y. Liu, L. Shao, L. Jiang, Simply realizing ‘‘water diode’’ Janus membranes for multifunctional smart applications, Mater. Horiz. 4 (2017) 701-708.

[15] X. Yang, Z. Wang, L. Shao, Construction of oil-unidirectional membrane for integrated oil collection with lossless transportation and oil-in-water emulsion purification, J. Membr. Sci. 549 (2018) 67-74.

[16] B. Shang, Y. Wang, B. Peng, Z. Deng, Bioinspired polydopamine particles-assisted construction of superhydrophobic surfaces for oil/water separation, J. Colloid Interf. Sci. 482 (2016) 240-251.

[17] W. Zhang, N. Liu, Y. Cao, Y. Chen, L. Xu, X. Lin, L. Feng, A solvothermal route decorated on different substrates: controllable separation of an oil/water mixture to a stabilized nanoscale emulsion, Adv. Mater. 27 (2015) 7349-7355.

[18] Q. Zhang, Y. Cao, N. Liu, W. Zhang, Y. Chen, L. Feng, A facile approach for fabricating dual-function membrane:

Simultaneously removing oil from water and adsorbing water-soluble proteins, Adv. Mater. Interfaces 3 (2016) 1600291.
[19] F. Chen, J. Song, Z. Liu, J. Liu, H. Zheng, J. Sun, W. Xu, X. Liu, Atmospheric pressure plasma functionalized polymer mesh: An environmentally friendly and efficient tool for oil/water separation, ACS Sustainable Chem. Eng. 4 (2016) 6828-6837.
[20] R.A. Ortega, E.S. Carter, A.E. Ortega, Nylon 6,6 nonwoven fabric separates oil contaminates from oil-in-water emulsions, PLOS ONE 11(7) (2016) e0158493.
[21] M.A. Gondal, M.S. Sadullah, M.A. Dastageer, G.H. McKinley, D. Panchanathan, K.K. Varanasi, Study of factors governing oil−water separation process using TiO_2 films prepared by spray deposition of nanoparticle dispersions, ACS Appl. Mater. Interfaces 6 (2014) 13422-13429.
[22] X. Tian, V. Jokinen, J. Li, J. Sainio, R.H.A. Ras, Unusual dual superlyophobic surfaces in oil–water systems: The design principles, Adv. Mater. 28 (2016) 10652-10658.
[23] S. Michielsen, H.J. Lee, Design of a superhydrophobic surface using woven structures, Langmuir 23 (2007) 6004-6010.
[24] A. Tuteja, W. Choi, J.M. Mabry, G.H. McKinley, R.E. Cohen, Robust omniphobic surfaces, PNAS 105(47) (2008) 18200-18205.
[25] Z. Wang, X. Jiang, X. Cheng, C.H. Lau, L. Shao, Mussel-inspired hybrid coatings that transform membrane hydrophobicity into high hydrophilicity and underwater superoleophobicity for oil-in-water emulsion separation, ACS Appl. Mater. Interfaces 7 (2015) 9534-9545.
[26] C. Journet, S. Moulinet, C. Ybert, S.T. Purcell, L. Bocquet, Contact angle measurements on superhydrophobic carbon nanotube forests: Effect of fluid pressure, Europhys. Lett. 71 (2005) 104-109.
[27] Z. Xue, S. Wang, L. Lin, L. Chen, M. Liu, L. Feng, L. Jiang, A novel superhydrophilic and underwater superoleophobic hydrogel-coated mesh for oil/water separation, Adv. Mater. 23 (2011) 4270-4273.
[28] A. Lafuma, D. Quéré, Superhydrophobic States, Nat. Mater. 2 (2003) 457-460.
[29] J.W. Grate, K.J. Dehoff, M.G. Warner, J.W. Pittman, T.W. Wietsma, C. Zhang, M. Oostrom, Correlation of oil−water and air−water contact angles of diverse silanized surfaces and relationship to fluid interfacial tensions, Langmuir 28 (2012) 7182-7188.
[30] R.N. Wenzel, Resistance of solid surfaces to wetting by water, Ind. Eng. Chem. 28 (8) (1936) 988-994.
[31] A.B.D. Cassie, S. Baxter, Wettability of porous surfaces, Trans. Faraday Soc. 40 (1944) 546-551.
[32] Y.C. Jung, B. Bhushan, Wetting behavior of water and oil droplets in three-phase interfaces for hydrophobicity / philicity and oleophobicity / philicity, Langmuir 25 (2009) 14165-14173.
[33] A. Tuteja, W. Choi, M. Ma, J.M. Mabry, S.A. Mazzella, G.C. Rutledge, G.H. McKinley, R.E. Cohen, Designing superoleophobic surfaces, Science 318 (2007) 1618-1622.
[34] X. Gao, L. Xu, Z. Xue, L. Feng, J. Peng, Y. Wen, S. Wang, X. Zhang, Dual-scaled porous nitrocellulose membranes with underwater superoleophobicity for highly efficient oil/water separation, Adv. Mater. 26 (2014) 1771-1775.
[35] P. Zhang, S. Wang, S. Wang, L. Jiang, Superwetting surfaces under different media: effects of surface topography on wettability, Small 11(16) (2015) 1939-1946.
[36] A. Marmur, From hygrophilic to superhygrophobic: Theoretical conditions for making high-contact-angle surfaces from low-contact-angle materials, Langmuir 24 (2008) 7573-7579.
[37] K. Acatay, E. Simsek, C. Ow-Yang, Y.Z. Menceloglu, Tunable, superhydrophobically stable polymeric surfaces by electrospinning, Angew. Chem. Int. Ed. 43 (2004) 5210-5213.
[38] A. Marmur, Wetting on hydrophobic rough surfaces: To be heterogeneous or not to be? Langmuir 19 (2003) 8343-8348.
[39] N.A. Patankar, On the modeling of hydrophobic contact angles on rough surfaces, Langmuir 19 (2003) 1249-1253.
[40] J. Bico, U. Thiele, D. Quéré, Wetting of textured surfaces, Colloids Surf. A Physicochem. Eng. Asp. 206 (2002) 41-46.

Highlights

- Unmodified polyamide 6.6, rarely studied for oil removal, separated oil/water
- 2D mesh and 3D nonwoven polyamide were systematically studied for oil removal
- Roles of 2D and 3D porous structures in intrusion pressures were illustrated
- Different contact angles determined intrusion pressures of 2D mesh and 3D nonwoven
- 3D netting was beneficial for oil/water separation in terms of intrusion pressures

Graphical abstract